



Visualization of convection in a simulated gradient freeze cell during centrifugation

Peter V. Skudarnov, Liya L. Regel*, William R. Wilcox

International Center for Gravity Materials Science and Applications, Clarkson University, Potsdam, New York 13699-5814, USA

Received 19 February 1998; accepted 8 May 1998

Abstract

Experiments were performed in a simulated gradient freeze cell in order to reveal the effect of centrifugation on the convection in the cell. A laser light-cut technique was used for flow visualization. Flow patterns were observed in one vertical and two horizontal cross sections of the cell. Flow velocities were measured via particle displacement tracking velocimetry. Five centrifuge rotation rates ω were studied: 10, 15, 20, 30, and 40 rpm. A flow mode transition was found at a ω of about 30 rpm, which is in agreement with the theoretical prediction of Arnold [9]. A flow pattern observed in the vertical plane agrees qualitatively with the one calculated by Friedrich et al. [6,11]. The mean flow velocity in the bottom part of the test cell decreased beyond a rotation rate of 20 rpm, suggesting that a minimum might occur at a rotation rate higher than 40 rpm. © 1998 Elsevier Science B.V. All rights reserved.

1. Introduction

Convection in the melt during directional solidification greatly affects dopant distribution and the structural perfection of the resulting crystals. One of the methods to influence this convection is to perform the solidification in a centrifuge. The first experiments on gradient freeze crystal growth in a centrifuge in the thermally stable configuration were performed by Regel and Rodot [1–4]. In those experiments, a uniform axial dopant distribution was obtained in crystals grown at a particular net acceleration level. The effect was attributed to the

suppression of convection in the melt. The acceleration needed to obtain uniform doping was different for two different centrifuge arm lengths, while the rotation rate was the same. Several simple explanations have been given for the apparent minimum in convection observed in centrifuge experiments [1–6]. Recently, Wilcox et al. [7] compared the predictions of these models with the experiments and numerical simulations. They divided the models into three groups: Buoyancy–Coriolis balance, thermal stability, and flow transition. It was shown that none of the models agreed completely with all experimental data and numerical simulations.

To verify the predictions of the above theoretical models, a simulated gradient freeze cell was made out of transparent plastic. The cell was filled with

* Corresponding author. Fax: +1 315 268 3833; e-mail: regel@agent.clarkson.edu.

water (Prandtl number ≈ 6) seeded with tracer particles in order to visualize convection. Particle displacement tracking velocimetry (PDTV) was used for quantitative analysis of the flows. Arnold [9] showed numerically that in the present thermally stable configuration, the flow patterns developed in a low Prandtl number liquids (e.g. semiconductor melts) are similar to those in the high Prandtl number water. Our own numerical simulations show that similar flow patterns arise in water and liquid InSb, except the maximum flow velocity is about 2.5 times larger in InSb than in water.

When the parameters of our experiments are used, a flow transition [8,9] is expected at a centrifuge rotation rate of 22 rpm if the radial temperature difference is equal to 1°C . The ideal interface predicted by the thermal stability model [7–10] for our centrifuge at this rotation rate is essentially flat, i.e. $h_{\text{max}} \approx 0.03 \text{ mm}$ (see nomenclature). Predictions using Friedrich et al.'s [6,11] and Urpin's [12] scaling analyses for the Buoyancy–Coriolis balance model are shown in Fig. 1. Friedrich et al.'s analysis predicts a minimum in the flow velocity at a rotation rate of about 22 rpm. Urpin's order of magnitude analysis predicts a minimum in the convective velocity at a rotation rate of 28 rpm. These predictions caused us to perform experiments at rotation rates in the range of 10–40 rpm ($N = 1.02\text{--}3.63$ times earth's gravity).

2. Experimental equipment

Our experiments were performed on our High-Inertia Rotating Behemoth (HIRB) centrifuge at Clarkson University [13]. The centrifuge has an arm length of 1.5 m. A swing bucket for housing test equipment is attached to the centrifuge arm.

To simulate convective flows in the gradient freeze crystal growth technique, a newly redesigned test cell was used. The important difference of the new test cell from that used previously [14] is the introduction of a transparent cooling chamber to permit viewing from below. The chamber was attached to the bottom of the cell and was cooled by flowing cold water. The cooling system together with the test cell is shown schematically in Fig. 2. As in the previous experiments [14], a resistance

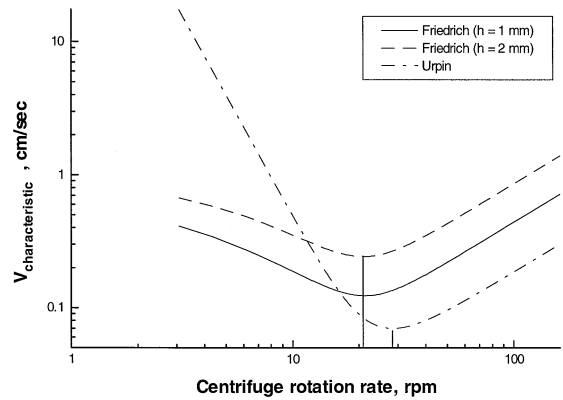


Fig. 1. Predictions of Friedrich et al.'s [11,16] and Urpin's [12] scaling analyses for our experiments. Parameters of HIRB centrifuge [13] and our test cell were used for calculations: (—) Friedrich et al. for a bottom end cap height $h = \pm 1 \text{ mm}$; (---) Friedrich et al. for a bottom end cap height $h = \pm 2 \text{ mm}$; (- · -) Urpin.

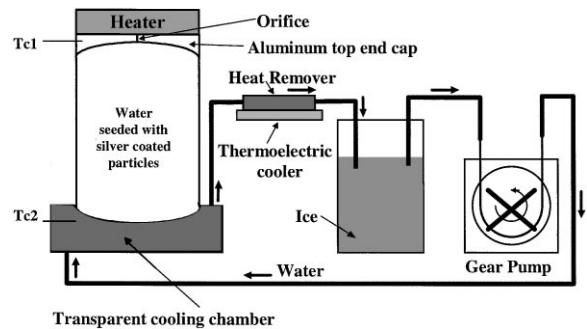


Fig. 2. Schematic diagram of the test cell and the cooling system.

heater at the top of the cell was used to establish a so-called thermally stable temperature field (temperature increasing with height) in the cell.

The shape of the crystal–melt interface in the thermally stable gradient freeze technique is normally concave [15]. Thus, to model the interface in our experiments, the shape of the bottom plastic end cap of the cell was also concave. The height used in this work was 1 mm. This particular height was chosen because it was expected to produce a radial temperature difference of about 1°C near

the bottom of the cell. We also used a cell with a flat bottom for comparison.

The test cell was filled with distilled water seeded with silver-coated [16] W-1000 Z-light microspheres (Zeelan Industries, Inc.). A laser light-cut technique was employed for observations of the convective flows. This technique has been described in detail elsewhere [14].

Particle displacement tracking velocimetry (PDTV) belongs to the family of particle imaging velocimetry techniques [17], and was used here for flow velocity determinations. This technique is based on analysis of a sequence of flow images. In our case, a sequence of four images was grabbed with a DT3955 [18] frame grabber from a videotape recorded during an experiment. This sequence was then analysed with Global Lab Image (Data Translation, Inc.) software to yield the coordinates of all particle centroids. The displacements of the tracer particles were found using a computer code that implemented the algorithm developed by Wernet [19]. From the velocity vectors at particle locations, the velocity vectors at regular grid points were interpolated as described by Ushijima [20]. Two sources of error are present in the PDTV measurements. These are the particle positioning error and the time interval error. The time interval error is negligible because the sequence of images was acquired with the frame grabber board programmed by the computer. Thus, the velocity measurement error σ_u arises from the error of particle centroid estimates [19,21]:

$$\frac{\sigma_u}{U} = \frac{\sigma_x}{X}, \quad (1)$$

where U is the mean value of the measured velocity, X is the total particle displacement from the first image to the last, and σ_x is the error in the total particle displacement. Assuming a particle centroid estimation error of ± 0.5 pixel, the total displacement error is $\sigma_x = \sqrt{1/2 + 1/2} = 1/\sqrt{2}$ pixels. Thus, for the worst case of a total displacement of only 3 pixels (only one pixel between two subsequent frames) the relative error in the measured velocity would be $\sigma_u/U = 0.23$. On average, in our experiments the relative error ranged from 0.1 to 0.14.

3. Results

3.1. Temperature measurements

To check the axisymmetry of the temperature field in the cell, the temperature was measured with four thermocouples (K-type, stainless steel sheathed, 0.01" diameter) placed around the perimeter of a horizontal cross section in the middle of the cell (Tc1–Tc4 in Fig. 3a). Measurements showed that the temperature field in this cross section was axisymmetric; the differences in the thermocouples readings were within the measurement error of 0.5°C. Similar results were observed when the thermocouples were placed in a horizontal cross section 6 mm¹ above the bottom end cap (Tc1'–Tc4' in Fig. 3a). From these measurements, it follows that the temperature field in the cell was axisymmetric and not measurably dependent on the centrifuge rotation rate up to 40 rpm, within experimental error.

For the measurements of the radial temperature difference at the edge of the end cap, one thermocouple was inserted through the cell wall with its tip near the inner surface of the wall. The other thermocouple was also inserted through the wall and its tip was positioned on the axis of the cell, as shown in Fig. 3b. The radial temperature difference measured in the experiments was approximately 1.8°C. The radial temperature difference at the edge of the bottom end cap can be estimated from the top and bottom temperatures and the geometrical dimensions of the cell as follows [11]:

$$\Delta T_r = (T_{\text{top}} - T_{\text{bottom}}) \cdot \frac{h}{l}, \quad (2)$$

where ΔT_r is the radial temperature difference, T_{top} is the temperature at the top, T_{bottom} is the temperature at the bottom, h is the bottom end cap height, and l is the length of the test cell. Using the experimental values for the top and bottom temperatures the radial temperature difference at the

¹ Throughout this paper, the height given for a horizontal cross-sectional plane is from the edge of the bottom end cap (see nomenclature). The distance from the center of the end cap would be 1 mm higher, because the end cap height is 1 mm.

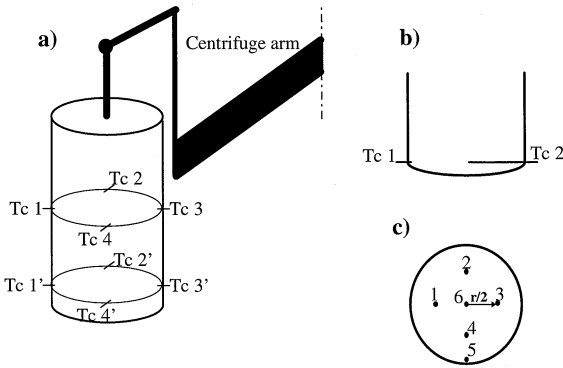


Fig. 3. Thermocouple positions in the cell.

edge of the bottom end cap (1 mm above the center of the end cap) was estimated from Eq. (2) to be 1.1°C. The discrepancy between the measured and estimated values can be attributed to the mispositioning of the central thermocouple. No dependence of the measured radial temperature difference on the centrifuge rotation rate was found.

The axial temperature profile in the cell was measured with a translated thermocouple without centrifugation. Fig. 4 shows the temperature along the axis measured every 1 mm, using a micrometer. The resulting temperature profile is almost linear.

To ensure that the curved bottom end cap was isothermal, a set of experiments was performed with several thermocouples (bare K-type, wire diameter 0.01") placed at the bottom of the cell. The tips of the thermocouples were positioned as shown in Fig. 3c. The differences in the thermocouple readings were within the measurement error of 0.5°C, confirming that the surface of the bottom end cap was nearly isothermal.

3.2. Convection patterns

Convection was viewed in three different planes inside the cell. One was horizontal 10 mm above the bottom end cap. Another was horizontal 3 mm above the bottom end cap. The third viewing plane was vertical passing through the cell's longitudinal axis. The positions of the viewing planes and the test cell relative to the centrifuge axis of rotation are

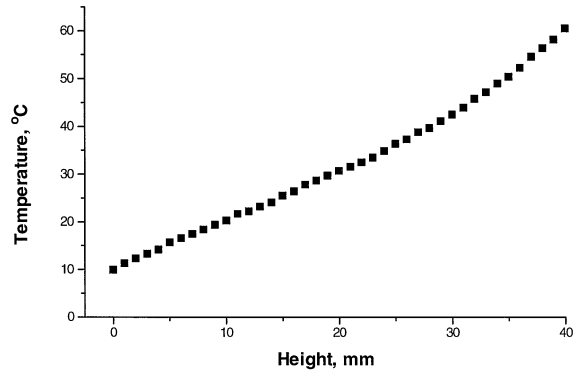


Fig. 4. Axial temperature profile inside the cell measured without centrifugation. End cap height 1 mm. Height measured from the center of the interface.

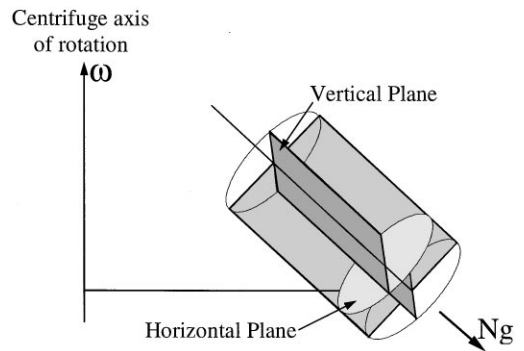


Fig. 5. Positions of the horizontal and vertical planes in the test cell relative to the centrifuge axis of rotation.

shown in Fig. 5. In each plane, the flow pattern was observed at five different centrifuge rotation rates: 10, 15, 20, 30, and 40 rpm.

In the horizontal plane 10 mm above the bottom (plane 1) the flow pattern was the same at all rotation rates. This flow pattern consisted of a single vortex occupying the entire cell cross section and rotating in the same direction as the centrifuge (see Fig. 6). Here, this rotation sense is referred to as counterclockwise, because the particles in this vortex moved counterclockwise on the video monitor. The flow in this cross section was inward, i.e. toward the cell axis.

In the horizontal plane 3 mm above the bottom (plane 2) the flow pattern changed with increasing

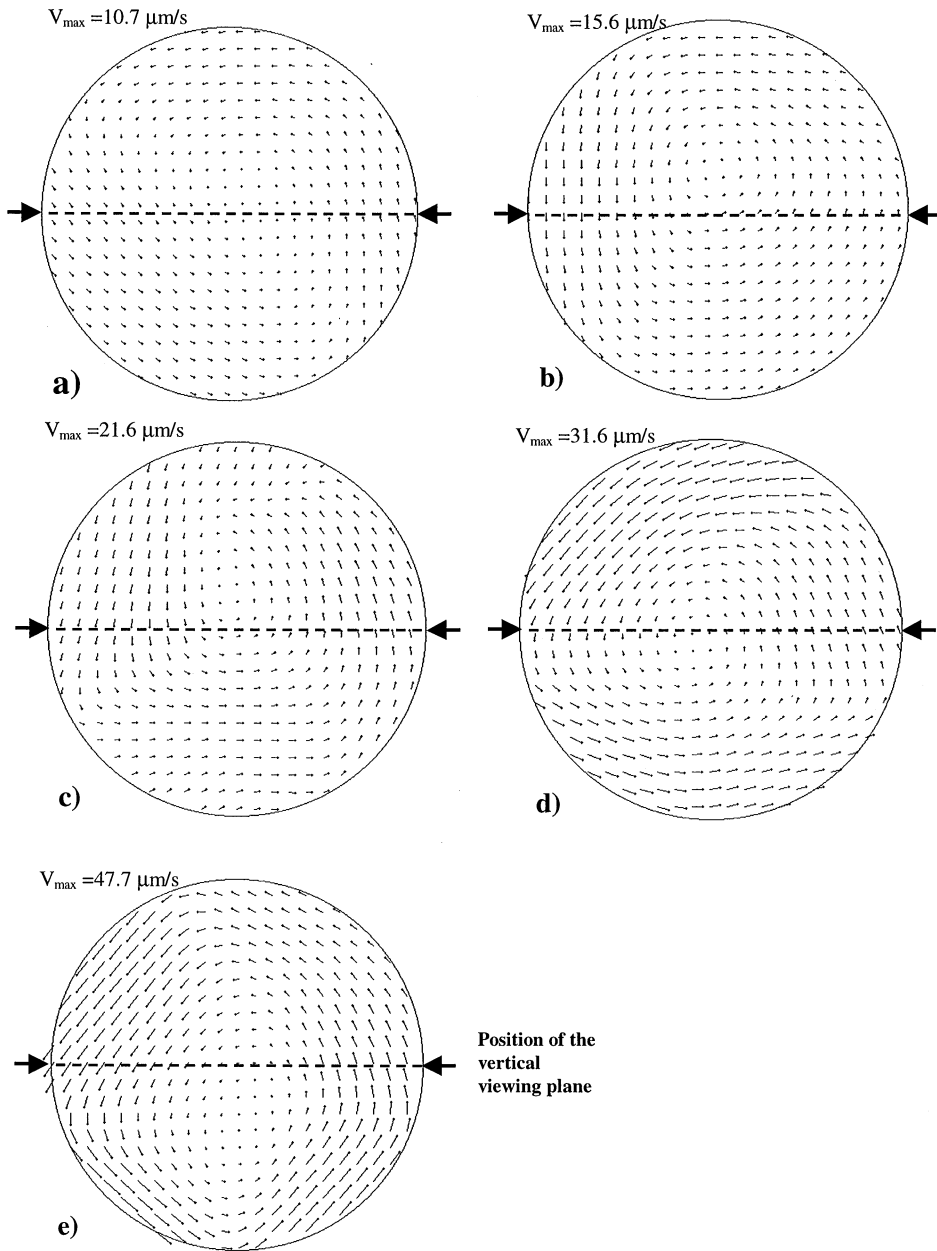


Fig. 6. Flow patterns in the horizontal plane positioned 10 mm above the bottom end cap. Interpolated from the measured particle velocities. The length of the arrow is proportional to the flow velocity. Centrifuge rotation rate: (a) 10 rpm; (b) 15 rpm; (c) 20 rpm; (d) 30 rpm; (e) 40 rpm.

rotation rate as shown in Fig. 7. For rotation rates of 10, 15 and 20 rpm, the flow pattern consisted of a single clockwise rotating vortex occupying the entire cross section. The flow in this cross section

was outward, i.e. toward the cell wall. At 30 rpm, two small secondary counterclockwise vortices appeared in the first and third quadrants of the cross section near the cell wall. These vortices

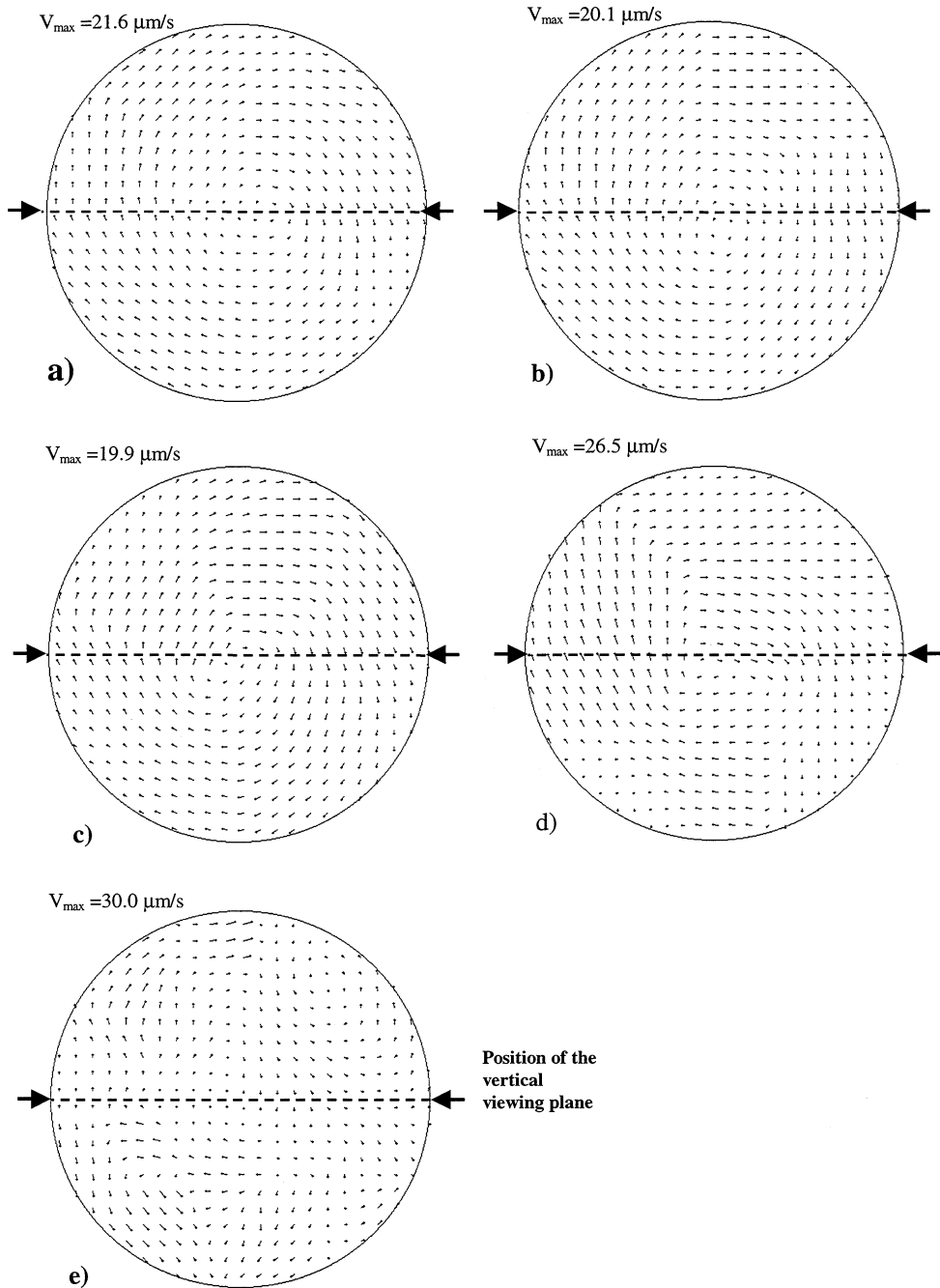


Fig. 7. Flow patterns in the horizontal plane positioned 3 mm above the bottom end cap. Interpolated from the measured particle velocities. The length of the arrow is proportional to the velocity. Centrifuge rotation rate (a) 10 rpm; (b) 15 rpm; (c) 20 rpm; (d) 30 rpm; (e) 40 rpm.

were small and not adequately resolved by the image processing software. Nevertheless, they were clearly observed on the time-lapse video record. At 40 rpm, there were four unequal vortices, one in each quadrant of the cross section. In the first, third, and fourth quadrant the vortices rotated counterclockwise, while in the second quadrant the vortex rotated clockwise. Without centrifuge rotation, the flow in plane 2 was radially outward, though it was not exactly axisymmetric. This is the basic flow, not affected by the Coriolis force. On the centrifuge, the Coriolis force deflects this flow and produces the clockwise rotating vortex observed at 10, 15 and 20 rpm.

The above experiments were repeated with a test cell having a flat bottom. At 3 mm above the bottom cap, the flow pattern was very similar to that in the cell with a curved bottom. At 10, 15 and 20 rpm, the flow pattern was again a single clockwise rotating vortex occupying the entire cross section. At 30 rpm, the flow pattern already changed to the four vortices type that is observed at 40 rpm with a curved bottom (Fig. 7e).

In the vertical plane in the cell with a curved bottom, the flow pattern changed a little with increasing rotation rate. The test cell can be conveniently divided into three vertical regions: bottom, central and top, according to the direction of the flow as shown in Fig. 8. There was a clockwise rotating flow along the bottom of the cell. Unfortunately, this flow was not captured by the image processing software for the following reason. This software considers only bright particles staying in the light sheet for at least 18 s (four frames with a time interval of 6 s). Particles staying in the light sheet for less than 18 s or twinkling particles (not visible on at least one frame) are disregarded by the tracking algorithm. In the bottom region, there were many particles moving from left to right slightly above the bottom. Unfortunately, there were only a few particles moving from right to left. In addition, the bottom end cap is concave; thus, it is impossible to observe from the side some particles moving close to the bottom. The above-mentioned clockwise rotating flow along the bottom was clearly visible on the time-lapse video recording of the convective pattern, but did not show up on flow patterns generated by the

image processing software. The bottom region was about 8 mm in height and its vertical size decreased only slightly with increasing centrifuge rotation rate.

In the central region all tracer particles moved almost horizontally, from right to left (Fig. 8). The height of this region decreased from about 17 to about 8 mm as the centrifuge rotation rate was increased from 10 to 40 rpm.

In the top region of the cell the tracer particles moved horizontally, from left to right. The height of this region increased from 17 to 28 mm with increasing rotation rate.

It is impossible to detect the direction of the circumferential component of a flow through observations in a vertical plane. In the vertical sheet, in our observations, most particles entered the light sheet, moved almost horizontally in the sheet, and then left the sheet. This entering and leaving behaviour indicates that particles had a component of velocity perpendicular to the vertical sheet – the circumferential flow observed in the horizontal planes. However, the direction of particle movement in the vertical plane does not tell the direction of flow in horizontal planes. Due to the slight nonaxisymmetry of the convective pattern, the axis of the circular flow can be in front of or behind the vertical observation plane. Depending on the position of this axis with respect to the vertical plane, opposite directions of flow in this plane could correspond to the same circular flow in a horizontal plane. This is shown schematically on the diagram in Fig. 9. Moreover, if the axis of a circular flow crosses the vertical plane, one would see in this vertical plane two regions with opposite directions of flow. This, we believe, was the case for our central and top regions. We came to this conclusion because in the vertical plane the directions of the flow were the same in all three regions in the experiments with the cell having a flat bottom.

From Fig. 8, it is seen that in the bottom and central regions the vertical component of the flow was much weaker than the horizontal component. Combining the results of observations in the vertical and horizontal planes, we conclude that the flow in the cell was mainly rotational about the axis of the cell. The flow in the bottom had an opposite rotation sense to that in the rest of the cell. In the

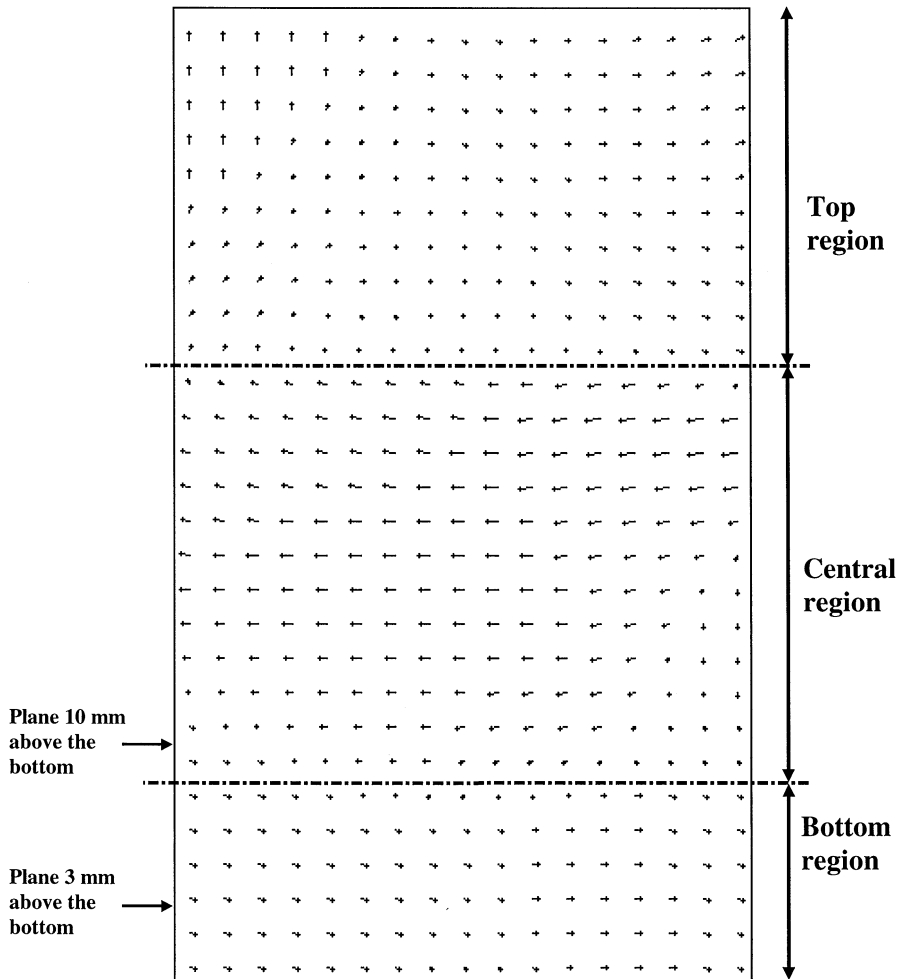


Fig. 8. Flow pattern in the vertical plane of the cell. Centrifuge rotation rate 15 rpm. Bottom end cap height 1 mm.

bottom region, in addition to the circular flow in the horizontal plane, there existed a clockwise rotating flow in the vertical plane. Increasing the centrifuge rotation rate did not change the flow pattern in the bulk of the cell, while in the bottom region there was a flow mode transition at about 30 rpm.

3.3. Flow velocity measurements

Flow velocities were measured using PDTV as described in Section 2.2. Mean velocities were obtained both from the measured velocity vectors at

particle positions, and from the velocity vectors interpolated at the grid points. Result of the flow velocity measurements in the planes 10 (plane 1) and 3 mm (plane 2) above the bottom end cap in the cells with flat and curved bottom cap are shown in Figs. 10–12. In plane 1, both mean and maximum flow velocity increase with increasing rotation rate (Fig. 10). In plane 2, there is a shallow minimum in the mean flow velocity at 15 rpm, and then the mean flow velocity decreases beyond 20 rpm (Figs. 11 and 12).

The mean flow velocity obtained from values measured at particle locations was always higher

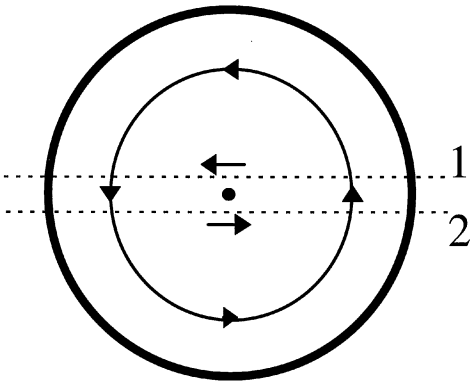


Fig. 9. Direction of flow observed in the vertical plane depends on the position of this plane (1 or 2) relative to the axis of the circular flow in the horizontal plane.

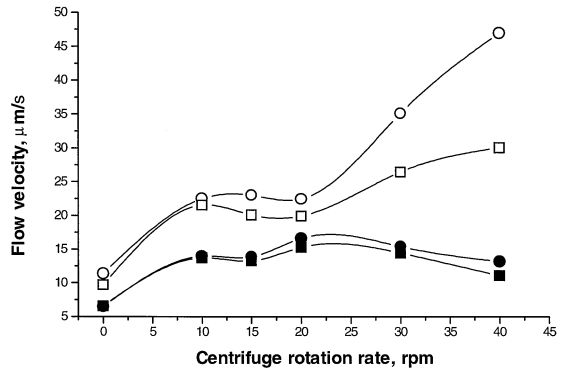


Fig. 11. Mean and maximum flow velocities ($\mu\text{m/s}$) measured in a horizontal cross section 3 mm above the bottom end cap of height 1 mm: (●) Mean flow velocity obtained from the measured values; (■) mean flow velocity obtained from the interpolated values; (○) maximum flow velocity obtained from the measured values; (□) maximum flow velocity obtained from interpolated values.

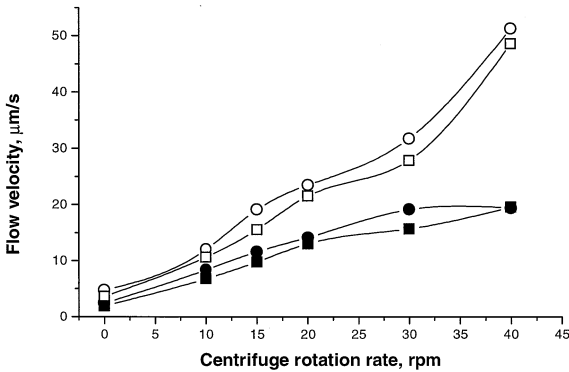


Fig. 10. Mean and maximum flow velocities ($\mu\text{m/s}$) measured in a horizontal cross section 10 mm above the bottom end cap of height 1 mm: (●) Mean flow velocity obtained from the measured values; (■) mean flow velocity obtained from the interpolated values; (○) maximum flow velocity obtained from the measured values; (□) maximum flow velocity obtained from the interpolated values.

than that obtained from interpolated values. This can be explained as follows. If we assume that all the particles move at the same velocity, then those moving parallel to the light sheet (plane of observation) would have the highest apparent velocity and the longest residence time within the sheet. The particles moving at a sharp angle to the light sheet would have the smallest apparent velocity. They also would be within the sheet for the shortest time, often too short for a velocity measurement. Thus, the particles with the slowest apparent velocity

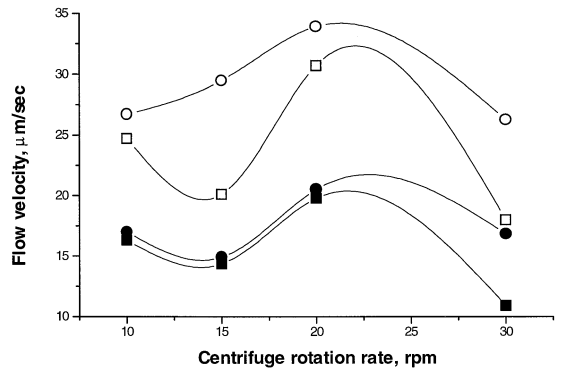


Fig. 12. Mean and maximum flow velocities ($\mu\text{m/s}$) measured in a horizontal cross section 3 mm above the bottom end cap. Flat bottom end cap: (●) Mean flow velocity obtained from the measured values; (■) mean flow velocity obtained from the interpolated values; (○) maximum flow velocity obtained from the measured values; (□) maximum flow velocity obtained from the interpolated values.

would be undercounted. Consequently, the interpolated values yield a more accurate measure of the mean apparent velocity.

4. Discussion

The flow pattern in the vertical plane numerically calculated by Friedrich et al. [7,9] is very

similar to that observed in our experiments. Unfortunately, they did not plot flow patterns in the horizontal planes, making it impossible to compare with our results.

The flow mode transition observed in the horizontal cross section 3 mm above the bottom end cap is in agreement with the theoretical prediction of Arnold [8,11]. A plot of Ad versus centrifuge rotation rate is shown in Fig. 13. It is seen that at the observed transition, the value of Ad was between 1 and 1.3. This transition was not detected in the side-view experiments. This illustrates the importance of end-view observations when dealing with convective flows on a centrifuge. Friedrich et al. [7,9] did not report a flow transition in their numerical simulation. However, they may have missed it because they displayed flow patterns only in the vertical plane and only for two different rotation rates.

In the horizontal plane 3 mm above the bottom, a shallow minimum in the mean flow velocity was found at a rotation rate of 15 rpm. The mean flow velocity decreased with increasing rotation rate beyond 20 rpm (Fig. 11), suggesting that a deeper minimum could occur at higher rotation rates. No minimum in the flow velocity was associated with the flow transition observed in this plane.

Similar flow patterns were observed at 10, 15 and 20 rpm in the horizontal cross section 3 mm

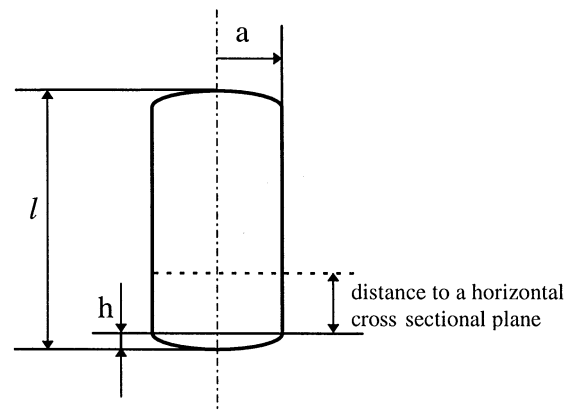
above the bottom in cells with flat and 1 mm height end caps. This leads us to the conclusion that the curvature of the end cap does not appreciably affect the flow in the cell at low rotation rates when the end cap height is 1 mm or less.

5. Conclusions

The flow pattern observed in the vertical plane in our test cell filled with water agrees well with that calculated by Friedrich et al. [7,9] for a germanium melt. The flow mode transition observed in our experiments occurs at about the rotation rate predicted by Arnold et al. [8,9]. The mean flow velocity in the horizontal plane 3 mm above the bottom of the cell decreased beyond a rotation rate of 20 rpm. This suggests that it is possible that a deep minimum in the flow velocity occurs at a higher rotation rate. Further numerical modeling, considering all aspects of centrifugal directional solidification, needs to be performed to reach a complete understanding of this complicated phenomenon.

Nomenclature

Test cell geometry



Dimensional quantities

a	radius of the test cell, m
C_p	specific heat of the liquid, J/kg K

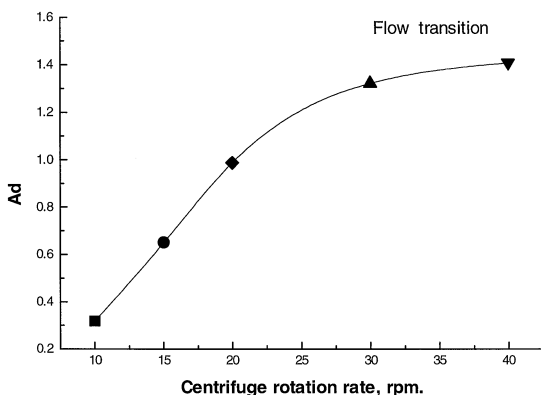


Fig. 13. Ad corresponding to the experiments with the test cell having a curved bottom. Symbols correspond to the flow patterns in a plane 3 mm above the bottom end cap shown in Fig. 7: (■) Fig. 9a; (●) Fig. 9b; (◆) Fig. 9c; (▲) Fig. 9d; (▼) Fig. 9e.

g	acceleration due to earth's gravity, 9.81 m/s ²
h	height of the concave bottom end cap, m
k	thermal conductivity of the liquid, J/m s K
l	length of the test cell, m
Ng	net acceleration g_{total} ; vector sum of g and $\omega^2 r_c$, with value of $\sqrt{g^2 + (\omega^2 r_c)^2}$, m/s ²
r_c	distance of the center of the bottom end cap from the centrifuge axis, m
T	temperature, K
μ	dynamic viscosity of the liquid, kg/m s
ω	centrifuge rotation rate, rad/s

Subscripts

a	axial value
bottom	value near the bottom of the cell
C	cold
H	hot
max	maximum value
r	radial value
top	value near the top of the cell

Nondimensional quantities

Arnold number	$Ad = \omega^2 l [T_H - T_C]_a / Ng [T_H - T_C]_r$ For constant axial gradient $Ad = \omega^2 l^2 / Ng h$
Prandtl number	$Pr = C_p \mu / k$

Acknowledgements

This research was supported by the National Science Foundation under grant number DMR-9414304. We thank Professor Gregory Campbell for the use of the video frame grabber and the image analysis software.

References

- [1] L.L. Regel, G.V. Sarafanov, A.M. Turtchaninov, Inst. Kosm. Issled. Akad. SSSR. Preprint No. 907, 1984. Cited in L.L. Regel, Materials Processing in Space, vol. 1, Consultants Bureau, New York, 1990.
- [2] L.L. Regel, G.V. Sarafanov, I.V. Videnskii, A.M. Turtchaninov, H. Rodot, Inst. Kosm. Issled. Akad. Nauk SSSR, Preprint No. 908, 1984. Cited in L.L. Regel, Materials Processing in Space, vol. 1, Consultants Bureau, New York, 1990.
- [3] H. Rodot, L.L. Regel, A.M. Turtchaninov, J. Crystal Growth 104 (1990) 280.
- [4] H. Rodot, L.L. Regel, G.V. Sarafanov, M. Hamidi, I.V. Videnskii, A.M. Turtchaninov, J. Crystal Growth 79 (1986) 77.
- [5] J. Friedrich, G. Muller, in: L.L. Regel, W.R. Wilcox (Eds.), Centrifugal Materials Processing, Plenum Press, New York, 1997, pp. 29–42.
- [6] J. Friedrich, J. Baumgartl, H.-J. Leister, G. Muller, J. Crystal Growth 167 (1996) 45.
- [7] W.R. Wilcox, L.L. Regel, W.A. Arnold, J. Crystal Growth 187 (1998) 543–558.
- [8] W.A. Arnold, W.R. Wilcox, F. Carlson, A. Chait, L.L. Regel, J. Crystal Growth 119 (1992) 24.
- [9] W.A. Arnold, Ph.D. Thesis, Clarkson University, 1993.
- [10] W.A. Arnold, L.L. Regel, in: L.L. Regel, W.R. Wilcox (Eds.), Materials Processing in High Gravity, Plenum Press, New York, 1994, pp. 17–34.
- [11] J. Friedrich, G. Muller, in: L.L. Regel, W.R. Wilcox (Eds.), Centrifugal Materials Processing, Plenum Press, New York, 1997, pp. 17–28.
- [12] V.A. Urpin, in: L.L. Regel, W.R. Wilcox (Eds.), Materials Processing in High Gravity, Plenum Press, New York, 1994, pp. 35–42.
- [13] R. Derebail, W.A. Arnold, G.J. Rosen, W.R. Wilcox, L.L. Regel, in: L.L. Regel, W.R. Wilcox (Eds.), Materials Processing in High Gravity, Plenum Press, New York, 1994, pp. 203–212.
- [14] P.V. Skudarnov, L.L. Regel, W.R. Wilcox, in: L.L. Regel, W.R. Wilcox (Eds.), Centrifugal Materials Processing, Plenum Press, New York, 1997, pp. 75–89.
- [15] D.H. Kim, R.A. Brown, J. Crystal Growth 109 (1991) 66.
- [16] T. Schmitt, J.N. Koster, H. Hamacher, Meas. Sci. Technol. 6 (1995) 682.
- [17] R.J. Adrian, Ann. Rev. Fluid Mech. 23 (1991) 261.
- [18] Data Translation DT3955 frame grabber, Data Translation, Technical Publications Department, 100 Locke Drive, Marlboro, MA 01752.
- [19] M.P. Wernet, Appl. Opt. 30 (1991) 1839.
- [20] S. Ushijima, H. Takeda, N. Tanaka, Nucl. Eng. Des. 132 (1991) 265.
- [21] M.P. Wernet, R.V. Edwards, Appl. Opt. 29 (1990) 3399.